LAWRENCE
LIVERMORE
NATIONAL
LABORATORY

LLNL-JRNL-821360

Analysis of the Reactive CO2 Surface Flux in Electrocatalytic Aqueous Flow Reactors

T. Y. Lin, S. E. Baker, E. B. Duoss, V. A. Beck

April 12, 2021

Industrial & Engineering Chemistry Research

Disclaimer

Analysis of the reactive CO_2 surface flux in electrocatalytic aqueous flow reactors

Tiras Y. Lin,* Sarah E. Baker, Eric B. Duoss, and Victor A. Beck*

Lawrence Livermore National Laboratory, Livermore, California 94550, United States

E-mail: lin46@llnl.gov; beck33@llnl.gov*

Abstract

We study how the mass transfer of a chemical species in shear flow is suppressed by the production of a second species that partially reacts away the first species. The second species is produced at the surface with the first species as a reactant. Our work is directly motivated by electrochemical CO_2 reduction in aqueous flow reactors, where OH^- molecules generated by the CO evolution reaction react away CO_2 molecules, ultimately inhibiting the mass transfer of CO_2 to the cathode surface. We derive a simple approximation of the Sherwood number, a dimensionless measure of the mass flux into the surface, as a function of the Péclet number, surface Damköhler number, and bulk Damköhler number, and we compare our approximation to numerical solutions of the governing equations. We find that in the diffusion-limited regime, the Sherwood number is well described by the classical Graetz Lévêque result reduced by a reaction factor due to the competing bulk reaction; with the stoichiometry relevant to electrochemical CO_2 reduction, this reaction factor is 1/2. While the model problem we solve provides insight into how OH^- production affects CO_2 mass transfer, experimental systems often involve more complex chemistry. We thus also show how a common buffered electrolyte, $KHCO_3$, affects our results.

1 Introduction

As the concentration of CO_2 continues to rise in our atmosphere, directly driving the harmful effects of global warming, the need for technologies to reduce the net amount of CO_2 emissions remains critical. To succeed, these technologies need to be economically viable,[1,2] and their strengths and limitations need to be well understood. Broadly, the strategies to curb CO_2 emissions belong to three classes:[3] reducing our reliance on power generation methods that create significant CO_2 emissions (decarbonization),[4,5] capturing and storing CO_2 (carbon sequestration),[6] and converting CO_2 to other useful products (carbon recycling).[3] The electrochemical reduction of CO_2 in aqueous flow reactors is emerging as an especially attractive route to recycle carbon.[7–11] Despite continued performance improvements, however, the central questions surrounding transport of the dissolved gases to the reactive surface still remain unresolved. Indeed, overcoming mass transport limitations has been a central focus of many recent reactor engineering and design efforts.[11–16]

Understanding mass transfer is critical for the design of continuous flow reactors. In a typical setup, CO_2 is dissolved in solution, and this solution is flowed past a cathode where the CO_2 reduction reaction and the hydrogen evolution reaction occur.[17–20] Both of these reactions generate an OH^- as a product for each electron transferred, thus changing the pH near the cathode surface; local changes in the pH can directly affect the performance of the CO_2 reduction reaction.[21] Additionally, because the extra OH^- reacts away CO_2, the production of OH^- can inhibit the CO_2 molecules from reaching the cathode surface, thereby reducing the mass flux of CO_2 onto the cathode. Supplying the reactive surface with CO_2 is critical to the performance of these reactors, but the seemingly paradoxical situation arises where greater flux of CO_2 to the surface leads to greater production of hydroxide, further decreasing surface transport. Though it is obvious that greater CO_2 flux will lead to greater overall reaction, the quantitative impact of hydroxide production on mass flux is still unclear. It is important to note that the aqueous flow reactor is not the only reactor configuration used for CO_2 reduction; modern designs often utilize the gas-diffusion electrode, where CO_2

in the vapor phase is fed to a porous catalyst in order to mitigate mass transfer limitations.[8] The mass transfer of CO_2 is also affected in this design by the production of OH^-,[11,12,22] but since the associated transport phenomena are not particularly well understood in either case, we focus our attention in this work on the aqueous flow reactor.

Beyond the application of electrochemical CO_2 conversion, the problem of mass transfer of a chemical species to a reactive surface in the presence of fluid flow is a classical problem broadly in engineering.[23] The problem was originally considered by Graetz[24] and Lévêque[25], and this style of problem has been extended to include a variety of other features. For example, considerable attention has been given to problems where the heterogeneous surface reaction is not perfectly reactive, leading to a Robin-type boundary condition as opposed to a Dirichlet-type boundary condition, and to situations where the reaction only occurs on a fraction of the surface, leading to a mixed boundary value-type problem.[26–32] Researchers have also considered the effect of a homogeneous reaction in the liquid on mass transfer.[33] Notably, Friedlander and Litt[34] and Acrivos[35] have investigated the case where a chemical species flows past a surface, which then forms a second species. In these works, this second species is assumed to instantaneously react with the first species, and as a result, the boundary between the regions where the species concentrations are nonzero is assumed to be infinitesimally thin. For homogeneous reaction rates that are finite, Friedlander and Keller[36] examined the structure of the reaction zone for a one-dimensional diffusion-reaction problem. Den Hartog and Beek[37] studied the effect of a second species partially reacting away the primary species via a homogeneous second order reaction in various flow types and reported on the asymptotic mass transfer performance with respect to the supplied concentration ratio of the two species. To date, however, to the authors' knowledge, there have not been studies specifically examining the effect of this second reactive species on the mass transfer of the primary species, where the production of the second species at the surface is directly proportional to the consumption of the first species. This particular situation is what occurs in CO_2 reduction.

To investigate how the production of OH^- affects the mass transfer of CO_2 in an aqueous flow reactor, we motivate our work through the following reactions,[38,39]

$$CO_2 + 2OH^- \rightarrow CO_3^{2-} + H_2O \qquad \text{in the bulk, with rate} \sim C_{CO_2} C_{OH^-}, \tag{1a}$$

$$CO_2 + H_2O + 2e^- \rightarrow CO + 2OH^- \qquad \text{on the surface, with rate} \sim C_{CO_2}, \tag{1b}$$

where C_i is the concentration of species i, representing the problem of CO_2 saturated water undergoing the CO evolution reaction on the cathode surface. First, in §2, we set up the mathematical framework of the problem and derive an approximate expression for the mass flux by considering the various resistances to mass transfer. In §3, we compare our approximation to numerical solutions of the governing advection-diffusion-reaction equations. Additionally, because CO_2 reduction is regularly performed in buffered electrolyte,[40] we describe how the use of a buffered electrolyte affects the mass transfer. Finally, we conclude in §4 by discussing possible extensions of our work.

2 Methodology

2.1 Problem statement

We investigate how the mass transfer of a species X_1 is affected by the production of a second species X_2 that partially reacts away X_1. The second species X_2 is produced from a surface reaction with X_1 as a reactant. Specifically, we consider the reactions

$$nX_1 + mX_2 \rightarrow \text{product}, \qquad \text{in the bulk, with rate} = k_b C_1 C_2, \tag{2a}$$

$$pX_1 \rightarrow qX_2, \qquad \text{on the surface, with rate} = k_s C_1, \tag{2b}$$

where n, m, p, and q are stoichiometric coefficients, k_b and k_s are bulk and surface reaction rate constants, and $C_1 = C_1(x, y)$ and $C_2 = C_2(x, y)$ are the concentrations of species X_1

and X_2, respectively.

In our approach, we keep our analysis general: the analysis in this work is applicable to systems that can be described by any bulk and surface reactions that are of the form given in equations (2a) and (2b). While the analysis is kept general, in this paper, we will provide discussion throughout for how our analysis can be applied to the motivating problem of CO_2 reduction. Specifically, note that the particular stoichiometry of $(n, m, p, q) = (1, 2, 1, 2)$ corresponds to the problem of CO_2 saturated water undergoing the CO evolution reaction on a cathode surface, where $X_1 = CO_2$ and $X_2 = OH^-$; in this application, k_s can be estimated with Tafel kinetics[39], i.e.

$$k_s = \frac{i_0}{2FC_1^{\text{ref}}} \exp\left(-\frac{\alpha F}{RT}\eta\right), \tag{3}$$

where F is the Faraday constant, R is the ideal gas constant, T is the temperature, C_1^{ref} is a reference concentration, and η is the surface overpotential. The exchange current density i_0 and charge transfer coefficient α can be determined by fitting to experimental data, and the factor of "2" arises, because two electrons are needed to convert each CO_2 molecule. Additionally, in this CO_2 application, k_b has been estimated by, e.g. Astarita et al.[41], to be $8.42 \times 10^3\,\text{L}\,\text{mol}^{-1}\,\text{s}^{-1}$. Note that the reverse bulk reaction has been neglected here since the OH^- concentration is expected to be high near the cathode surface, and the reaction given in equation (1a) is expected to be near irreversible (e.g., see Fukunaka et al.[42]); this will be further discussed in §3.3 in discussion of the buffered electrolyte. Far away from the reactive surface, $C_1 = C_1^\infty$ and $C_2 = 0$, and the two species diffuse with the same Brownian diffusion coefficient D. Since the Schmidt number $\text{Sc} = \nu/D$, where ν is the solvent viscosity, is typically very large in flow reactors – in other words, the concentration boundary layers are much thinner than the fluid momentum boundary layer – we consider these reactions occurring within a shear flow with shear rate $\dot{\gamma}$ over a reactive surface of length L. A schematic of the problem is shown in figure 1(a). An important quantity of interest here is

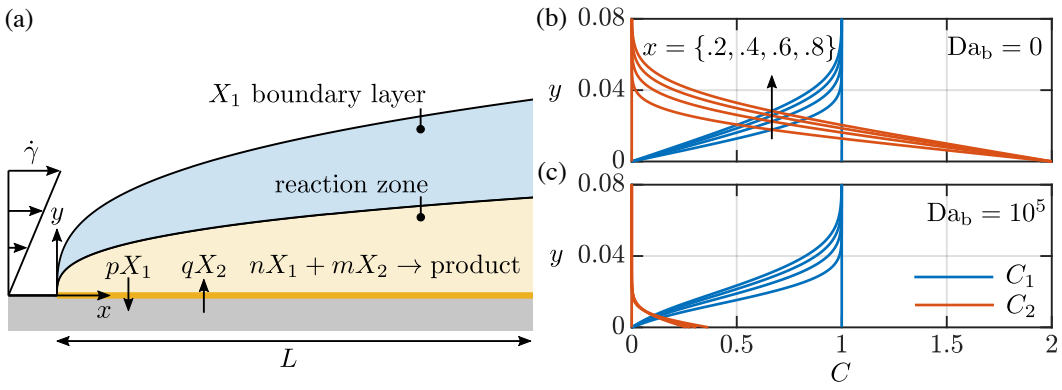

Figure 1: (a) Schematic of the problem considered. Species X_1 is advected past a reactive plate, where it is converted to species X_2. In the bulk, X_2 partially reacts away X_1. (b,c) Concentration profiles C_1 and C_2 are shown for the cases where $\mathrm{Da_b} = 0$ and $\mathrm{Da_b} = 10^5$, respectively, for the diffusion-limited case where $\mathrm{Da_s} = 10^6$; the Péclet number here is $\mathrm{Pe} = 10^5$, and the stoichiometry considered here is $(n, m, p, q) = (1, 2, 1, 2)$. Profiles are shown at several positions along the reactive surface, in increments of $\Delta x = 0.2$, including the boundary condition at $x = 0$, i.e., $C_1 = 1$ and $C_2 = 0$.

the averaged flux of C_1 into the reactive surface,

$$J = \frac{1}{L}\int_0^L D\frac{\partial C_1}{\partial y}(x, y = 0)\mathrm{d}x, \tag{4}$$

which is proportional to the CO current density in the CO_2 application.

We make our equations dimensionless with,

$$C_{\{1,2\}} = C_1^\infty C^*_{\{1,2\}}, \qquad x = Lx^*, \qquad y = Ly^*, \tag{5}$$

where the asterisk denotes a dimensionless quantity. This procedure yields the following dimensionless numbers,

$$\mathrm{Pe} = \frac{\dot{\gamma}L^2}{D}, \qquad \mathrm{Da_s} = \frac{k_\mathrm{s}L}{D}, \qquad \mathrm{Da_b} = \frac{k_\mathrm{b}L^2C_1^\infty}{D}, \tag{6}$$

where Pe is a Péclet number characterizing the strength of the shear flow and $\mathrm{Da_s}$ and $\mathrm{Da_b}$ are Damköhler numbers characterizing the strength of the surface and bulk reactions,

respectively. Hereafter, we omit the asterisk used to denote a nondimensional quantity in order to simplify the notation, unless otherwise noted (e.g., x now refers to the dimensionless x^* in equation (5)).

The concentration fields C_1 and C_2 are governed by the following dimensionless advection-diffusion-reaction equations,

$$\mathrm{Pe}\, y\frac{\partial C_1}{\partial x} = \frac{\partial^2 C_1}{\partial x^2} + \frac{\partial^2 C_1}{\partial y^2} - n\mathrm{Da_b} C_1 C_2, \qquad x, y \geq 0, \tag{7a}$$

$$\mathrm{Pe}\, y\frac{\partial C_2}{\partial x} = \frac{\partial^2 C_2}{\partial x^2} + \frac{\partial^2 C_2}{\partial y^2} - m\mathrm{Da_b} C_1 C_2, \qquad x, y \geq 0, \tag{7b}$$

$$C_{\{1,2\}} = \{1, 0\}, \qquad \text{at } x = 0, \tag{7c}$$

$$\frac{\partial C_{\{1,2\}}}{\partial y} = \{p, -q\}\mathrm{Da_s} C_1, \qquad \text{at } y = 0, \tag{7d}$$

$$C_{\{1,2\}} = \{1, 0\}, \qquad \text{at } y = \infty. \tag{7e}$$

Note that in the limit of $\mathrm{Da_s} \to \infty$, i.e. the so-called diffusion-limited regime, the boundary condition given in equation (7d) reduces to,

$$C_1 = 0, \qquad \frac{\partial C_2}{\partial y} = -\frac{q}{p}\frac{\partial C_1}{\partial y}, \qquad \text{at } y = 0. \tag{8}$$

Ultimately, we are interested in understanding how Pe, $\mathrm{Da_b}$, and $\mathrm{Da_s}$ affect the flux of C_1 through the reactive surface. We thus define an averaged Sherwood number, i.e. a dimensionless version of flux J, to be

$$\mathrm{Sh}(\mathrm{Pe}, \mathrm{Da_b}, \mathrm{Da_s}) = \frac{JL}{DC_1^\infty} = \int_0^1 \frac{\partial C_1}{\partial y}(x, y = 0)\mathrm{d}x, \tag{9}$$

and we expect the presence of C_2 to reduce Sh as it partially reacts away C_1. Sh is also related to the average surface concentration of C_1 due to the Robin boundary condition in equation (7d) as

$$\int_0^1 C_1(x, y = 0)\mathrm{d}x = \frac{1}{p\mathrm{Da_s}}\mathrm{Sh}(\mathrm{Pe}, \mathrm{Da_b}, \mathrm{Da_s}), \tag{10}$$

however, there is no analogous simple expression for C_2 due to the nature of the boundary condition. Additionally, note that it is also common engineering practice to report the dimensional flux based on a mass transfer coefficient k_m, so that, $J = k_\mathrm{m} C_1^\infty$. Our definition in equation (9) thus implies that $\mathrm{Sh} = k_\mathrm{m} L/D$.

In the CO_2 reduction community, it is also typical to present Sh as a percent utilization – i.e. the fraction of the input molar flux $C_1^\infty Q$, where Q is the volume flow rate of the input stream, that is used up by the surface reaction. In terms of Sh, the utilization is

$$\%\ \text{utilization} = 6\alpha^2 \mathrm{Pe}^{-1}\, \mathrm{Sh}(\mathrm{Pe}, \mathrm{Da_b}, \mathrm{Da_s}), \tag{11}$$

where $\alpha = L/h$, where h is the height of the channel in the y direction. This simple expression assumes that the local flux and velocity profile are uniform in the z direction, where the shear rate is approximated by $\dot{\gamma} = 6Q/(h^2 L_z)$ and L_z is the thickness of the reactive surface in the direction into the page. Note that for experimental systems, where Q is typically a pump input, this simple expression for $\dot{\gamma}$ can also be used to estimate the corresponding Péclet number Pe using equation (6).

In the following, we examine Sh and its dependence on the three dimensionless parameters Pe, $\mathrm{Da_b}$, and $\mathrm{Da_s}$, representing the strength of the flow, the strength of the bulk reaction, and the strength of the surface reaction, respectively. We first briefly review a known approximation when there is no bulk reaction in §2.2. Next, we propose a similar approximation when bulk reaction is included in §2.3. We solve equations (7a)-(7e) using a finite difference scheme implemented in Matlab and compare to our approximation in §3.

2.2 Approximation with no bulk reaction

When $\mathrm{Da_b} = 0$, the concentrations C_1 and C_2 are no longer coupled together, and it is sufficient to only consider equation (7a) along with the corresponding boundary conditions to determine Sh. Additionally, when $\mathrm{Da_s} = \infty$, and $\mathrm{Pe} \gg 1$, the problem reduces to the

well-known "Graetz Lévêque" problem, where the $\partial^2/\partial x^2$ term can be neglected, which has the similarity solution given by[37]

$$C_1(\eta) = \frac{3}{\Gamma(1/3)} \int_0^\eta \exp(-\sigma^3) \mathrm{d}\sigma, \tag{12a}$$

$$C_2(\eta) = \frac{q}{p} \left[1 - \frac{3}{\Gamma(1/3)} \int_0^\eta \exp(-\sigma^3) \mathrm{d}\sigma \right], \tag{12b}$$

where $\eta = y[\mathrm{Pe}/(9x)]^{1/3}$, and the Sherwood number is

$$\mathrm{Sh}_{\mathrm{GL}}(\mathrm{Pe}) = \mathrm{Sh}(\mathrm{Pe} \gg 1, \mathrm{Da_b} = 0, \mathrm{Da_s} = \infty) = \frac{9^{2/3}}{2\Gamma(1/3)} \mathrm{Pe}^{1/3}, \tag{13}$$

where the subscript "GL" stands for Graetz Lévêque. Note that in this limit, $C_1 = 0$ and $C_2 = q/p$ on the surface. Additionally, note that based on equation (11), the Graetz Lévêque problem gives a % utilization that scales like $\sim \mathrm{Pe}^{-2/3}$. It is also well-known that in the reaction-limited regime, where $\mathrm{Da_s} \ll 1$[28,29],

$$\mathrm{Sh}(\mathrm{Pe}, \mathrm{Da_b} = 0, \mathrm{Da_s} \ll 1) \approx \mathrm{Da_s}, \tag{14}$$

regardless of Pe, since $C_1 \approx 1$ and $C_2 \approx 0$ everywhere. Thus, an approximation can be formed for the case of general $\mathrm{Da_s}$ by summing together the associated mass transfer resistances in series[28,29] to be

$$\mathrm{Sh}(\mathrm{Pe} \gg 1, \mathrm{Da_b} = 0, \mathrm{Da_s}) \approx \left[\frac{1}{\mathrm{Da_s}} + \frac{1}{\mathrm{Sh}_{\mathrm{GL}}(\mathrm{Pe})} \right]^{-1}. \tag{15}$$

The same expression can also be derived by interpolating between the asymptotes using the expression given by Churchill and Usagi[43] where the asymptotes are weighted with a power of 1.

2.3 Approximation with bulk reaction

We aim to provide an approximation for the Sherwood number Sh for the case where $\mathrm{Da_b} > 0$ that is analogous to equation (15). We restrict our attention to the case where $\mathrm{Pe} \gg 1$, which is the regime relevant to CO_2 reduction. To first provide some intuition on the effect of bulk reaction, in figure 1(b,c), we show concentration profiles C_1 and C_2 at several x positions for the cases where $\mathrm{Da_b} = 0$ and $\mathrm{Da_b} = 10^5$, respectively, for the diffusion-limited case where $\mathrm{Da_s} = 10^6$; the Péclet number is fixed to $\mathrm{Pe} = 10^5$ here. When $\mathrm{Da_b} = 0$, the boundary layer of C_2 grows at exactly the same rate as the boundary layer of C_1, however, when $\mathrm{Da_b} \gg 1$, C_2 is quickly consumed by the bulk reaction with C_1, leading to depletion of C_1 near the reactive surface.

In figure 2, we show heat maps of the local bulk reaction rate, $C_1(x, y)C_2(x, y)$, for the cases where $\mathrm{Da_b} = \{1, 10^3\}$ and $\mathrm{Da_s} = \{1, 10, 10^6\}$; the Péclet number here is $\mathrm{Pe} = 10^5$. At the relatively small value of surface Damköhler number $\mathrm{Da_s} = 1$, we observe that the local bulk reaction rate is small, regardless of the bulk Damköhler number $\mathrm{Da_b}$; at small $\mathrm{Da_s}$, a relatively small amount of C_2 is produced, leading to a weak bulk reaction. This implies that in the surface reaction-limited regime,

$$\mathrm{Sh}(\mathrm{Pe}, \mathrm{Da_b}, \mathrm{Da_s} \ll 1) \approx \mathrm{Da_s}, \tag{16}$$

just as in the case where $\mathrm{Da_b} = 0$. As $\mathrm{Da_s}$ increases further, more C_2 is produced at the surface. Initially, the bulk reaction becomes most significant at $y = 0$, but as $\mathrm{Da_s}$ becomes large, C_1 becomes fully depleted at $y = 0$, leading to the maximum bulk reaction occurring at a finite distance away from $y = 0$. As $\mathrm{Da_b}$ increases, the local reaction rate depletes faster in the x direction, due to the reactants C_1 and C_2 being reacted away quicker.

We hypothesize that the Graetz Lévêque limit can be modified in the presence of bulk

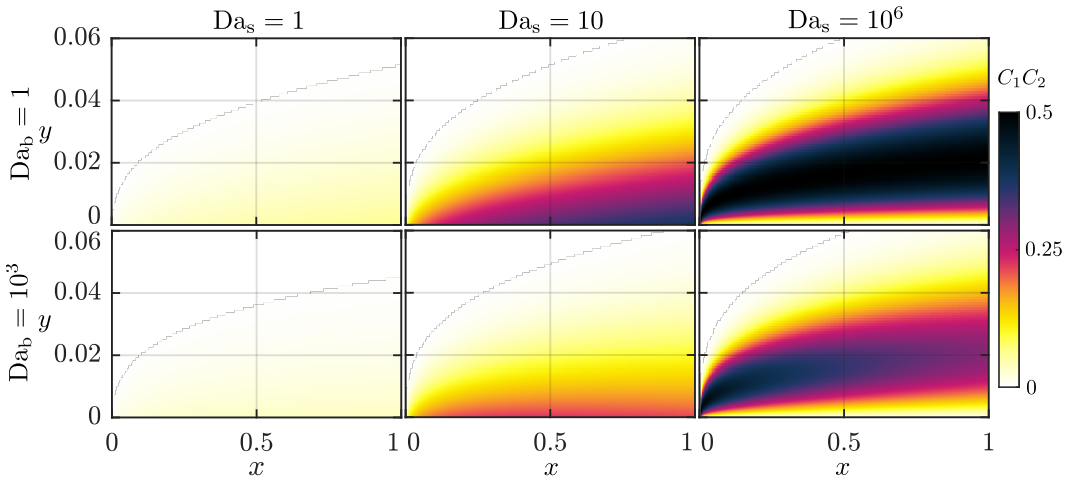

Figure 2: Local bulk reaction rate $C_1(x,y)C_2(x,y)$ is shown for cases where $\mathrm{Da_b} = \{1, 10^3\}$ and $\mathrm{Da_s} = \{1, 10, 10^6\}$. The Péclet number here is $\mathrm{Pe} = 10^5$ and the stoichiometry considered here is $(n, m, p, q) = (1, 2, 1, 2)$.

reaction to be of the form,

$$\mathrm{Sh}(\mathrm{Pe} \gg 1, \mathrm{Da_b}, \mathrm{Da_s} = \infty) \approx f(\mathrm{Pe}, \mathrm{Da_b})\mathrm{Sh_{GL}}(\mathrm{Pe}), \tag{17}$$

where the factor $f(\mathrm{Pe}, \mathrm{Da_b})$ can be determined by solving a one-dimensional diffusion-reaction problem from $y = 0$ to the averaged thickness of the C_1 boundary layer. Written in this way, $f(\mathrm{Pe}, \mathrm{Da_b})$ has also been called the "reaction factor",[37] i.e. the reduction in Sh due to bulk reaction in the diffusion-limited regime. This approach is akin to a film theory approach,[44] except here, we accurately account for the boundary layer growth. We define the local boundary layer thickness as the y coordinate where $C_1 = 1$ if the concentration gradient is assumed uniformly equal to the value at the wall, $\partial C_1/\partial y(x, y = 0)$, as given by the Graetz Lévêque problem; in the presence of bulk reaction, this remains valid since the boundary layer for C_2 can never exceed the boundary layer for C_1. This gives a local boundary layer thickness of $l_{\mathrm{BL}}(x) = \left[\Gamma(1/3)/3^{1/3}\right] \mathrm{Pe}^{-1/3} x^{1/3}$. Thus, the boundary layer

thickness averaged within $0 \leq x \leq 1$ is

$$L_{\mathrm{BL}} = \frac{3^{2/3}\Gamma(1/3)}{4}\mathrm{Pe}^{-1/3}. \tag{18}$$

Thus, to determine the reaction factor $f(\mathrm{Pe}, \mathrm{Da_b})$, i.e. the amount that the Sherwood number is reduced by compared to the case where $\mathrm{Da_b} = 0$, we solve the following set of ordinary differential equations,

$$\frac{\mathrm{d}^2 C_1^{\mathrm{1D}}}{\mathrm{d}\bar{y}^2} - n\mathrm{Da_b} L_{\mathrm{BL}}^2 C_1^{\mathrm{1D}} C_2^{\mathrm{1D}} = 0, \qquad 0 \leq \bar{y} \leq 1, \tag{19a}$$

$$\frac{\mathrm{d}^2 C_2^{\mathrm{1D}}}{\mathrm{d}\bar{y}^2} - m\mathrm{Da_b} L_{\mathrm{BL}}^2 C_1^{\mathrm{1D}} C_2^{\mathrm{1D}} = 0, \qquad 0 \leq \bar{y} \leq 1, \tag{19b}$$

$$C_1^{\mathrm{1D}} = 0, \qquad \frac{\mathrm{d}C_2^{\mathrm{1D}}}{\mathrm{d}\bar{y}} = -\frac{q}{p}\frac{\mathrm{d}C_1^{\mathrm{1D}}}{\mathrm{d}\bar{y}}, \qquad \text{at } \bar{y} = 0, \tag{19c}$$

$$C_{\{1,2\}}^{\mathrm{1D}} = \{1, 0\}, \qquad \text{at } \bar{y} = 1, \tag{19d}$$

where $\bar{y}$ has been scaled by L_{BL}, i.e. $\bar{y} = y/L_{\mathrm{BL}}$. We thus observe that the effective bulk Damköhler number for this auxiliary one-dimensional problem is $\mathrm{Da_{b,eff}} = \mathrm{Da_b} L_{\mathrm{BL}}^2$. We can then determine $f(\mathrm{Pe}, \mathrm{Da_b})$ to be

$$f(\mathrm{Pe}, \mathrm{Da_b}) = \frac{\mathrm{d}C_1^{\mathrm{1D}}}{\mathrm{d}\bar{y}}(\bar{y} = 0), \tag{20}$$

which is equal to 1 when $\mathrm{Da_b} = 0$. Our ansatz is that this one-dimensional problem within the averaged boundary layer can describe the Sherwood number for the two-dimensional problem, where the local flux is nonuniform over the wall. With the reaction factor $f(\mathrm{Pe}, \mathrm{Da_b})$, we can then form our full approximation. By again summing together the associated mass transfer resistances for the case where $\mathrm{Da_b} \ll 1$ given in equation (16) and the case where $\mathrm{Da_b} = \infty$ given in equation (17), we determine our proposed approximation for Sh for general $\mathrm{Da_s}$ and $\mathrm{Da_b}$ to be

$$\mathrm{Sh}(\mathrm{Pe} \gg 1, \mathrm{Da_b}, \mathrm{Da_s}) \approx \left[\frac{1}{\mathrm{Da_s}} + \frac{1}{f(\mathrm{Pe}, \mathrm{Da_b})\mathrm{Sh_{GL}}(\mathrm{Pe})}\right]^{-1}. \tag{21}$$

The analysis conducted thus far is directly relevant to flat plate electrodes in liquid-fed flow reactors, as shown in figure 1(a). Of course, there are other liquid-fed reactor configurations, e.g., non-planar electrodes, electrodes attached to a flow-field plate, porous electrodes. It is important to note that our analysis can be applied in some form to any reactor where there is electrolyte flow past a relatively flat reactive surface, because all fluid flows past a surface will locally look like the shear flow assumed in our work to a first approximation. In more complex geometries, equation (21) may not be directly applicable, but the resistances to mass transfer above could potentially be used within a more complex resistance model of mass transfer.

3 Results and discussion

3.1 Reduction of Graetz Lévêque flux due to bulk reaction

We first demonstrate that equation (17) is a reasonable approximation of Sh in the diffusion-limited regime where $\mathrm{Da_s} \gg 1$. In figure 3, we show the factor $f(\mathrm{Pe}, \mathrm{Da_b})$, determined through numerical solution of one-dimensional equations (19a)-(19d), plotted against the effective bulk Damköhler number $\mathrm{Da_{b,eff}} = \mathrm{Da_b} L_{\mathrm{BL}}^2$. By considering a perturbation expansion and stoichiometric balance when $\mathrm{Da_{b,eff}} \ll 1$ and $\mathrm{Da_{b,eff}} \to \infty$, respectively, we also have the following approximate expressions,

$$f(\mathrm{Pe}, \mathrm{Da_b}) = \begin{cases} 1 + A_1 \mathrm{Da_{b,eff}} + A_2 \mathrm{Da_{b,eff}}^2 + A_3 \mathrm{Da_{b,eff}}^3 + \ldots, & \mathrm{Da_{b,eff}} \ll 1, \\ \dfrac{mp}{mp+nq}, & \mathrm{Da_{b,eff}} \to \infty, \end{cases} \tag{22}$$

where $A_1 = -nq/(12p)$, $A_2 = nq(13mp + 15nq)/(1260p^2)$, and $A_3 = -nq(238m^2p^2 + 641mnpq + 379n^2q^2)/(181440p^3)$. In figure 3, we also show the analogous result calculated from two-dimensional simulations; the symbols show $\mathrm{Sh}(\mathrm{Pe}, \mathrm{Da_b}, \mathrm{Da_s})/\mathrm{Sh}(\mathrm{Pe}, \mathrm{Da_b} = 0, \mathrm{Da_s})$ for simulations conducted at $\mathrm{Pe} = 10^{\{5, 5.33, \ldots, 7\}}$ at the diffusion-limited regime of $\mathrm{Da_s} = 10^6$.

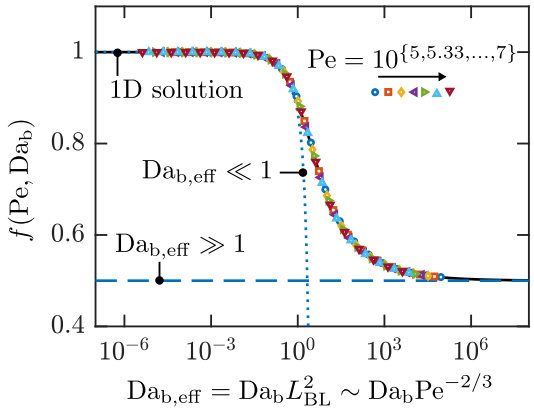

Figure 3: The factor $f(\mathrm{Pe}, \mathrm{Da_b})$, determined through solution of one-dimensional equations (19a)-(19d), is plotted against the effective bulk Damköhler number $\mathrm{Da_{b,eff}} = \mathrm{Da_b} L_{\mathrm{BL}}^2$ as a solid black line. The dotted and dashed lines indicate the perturbation theory result for small $\mathrm{Da_{b,eff}}$ and asymptotic result for large $\mathrm{Da_{b,eff}}$, respectively. The symbols show $\mathrm{Sh}(\mathrm{Pe}, \mathrm{Da_b}, \mathrm{Da_s})/\mathrm{Sh}(\mathrm{Pe}, \mathrm{Da_b} = 0, \mathrm{Da_s})$ calculated from two-dimensional simulations conducted at $\mathrm{Pe} = 10^{\{5,5.33,\ldots,7\}}$ at the diffusion-limited regime of $\mathrm{Da_s} = 10^6$. The stoichiometry considered here is $(n, m, p, q) = (1, 2, 1, 2)$.

The agreement between the two-dimensional simulations with the simple one-dimensional model illustrates that the factor $f(\mathrm{Pe}, \mathrm{Da_b})$ provides a good approximation of Sh in the diffusion-limited regime. Notably, for the problem of CO_2 saturated water undergoing the CO evolution reaction, $f(\mathrm{Pe}, \mathrm{Da_b}) = 1/2$ as $\mathrm{Da_{b,eff}} \to \infty$.

3.2 Use of approximation at general bulk and surface reaction strengths

In the previous subsection, we demonstrated that equation (17) is a reasonable approximation of Sh in the diffusion-limited regime where $\mathrm{Da_s} \gg 1$. We now proceed to examine whether or not the simple expression given in equation (21) – derived by simple summation of the mass transfer resistances – holds in the presence of bulk reaction.

In figure 4(a,b), we show the Sherwood number Sh calculated using two dimensional simulations along with our approximation given in equation (21) for various values of bulk Damköhler number $\mathrm{Da_b}$. In figure 4(a), Sh is plotted against the Péclet number Pe when the surface Damköhler number $\mathrm{Da_s}$ is 10^6, i.e. the diffusion-limited regime. We observe that

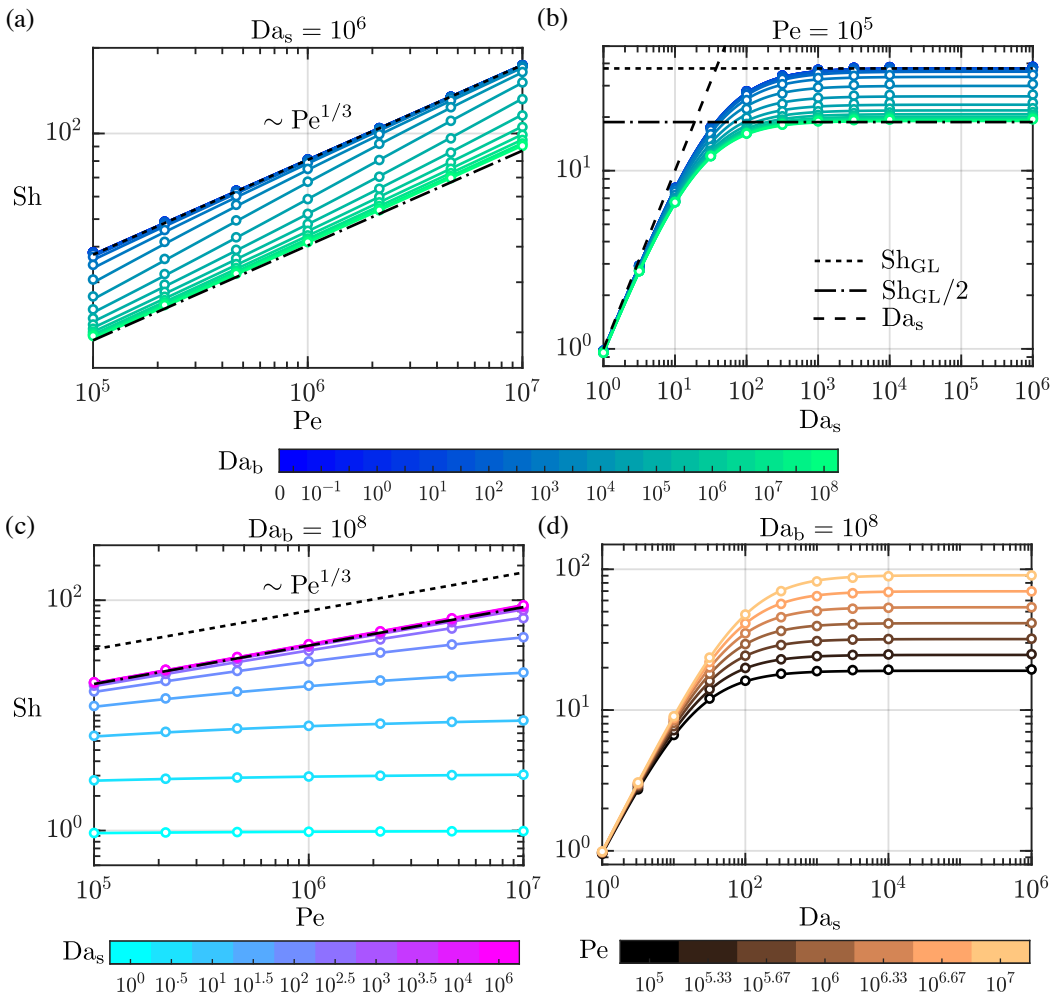

Figure 4: The Sherwood number Sh is plotted both from two dimensional simulations (∘) and with our approximation given in equation (21) (—). In panels (a,b), Sh is plotted for various values of the bulk Damköhler number $\mathrm{Da_b}$ as a function of (a) the Péclet number Pe when the surface Damköhler number $\mathrm{Da_s}$ is 10^6 and (b) $\mathrm{Da_s}$ when $\mathrm{Pe} = 10^5$. In panel (a), the scaling with $\mathrm{Pe}^{1/3}$ is demonstrated for the cases when $\mathrm{Da_b} = 0$ and $\mathrm{Da_b} \to \infty$, and in panel (b), the various limiting values of Sh are shown. In panels (c,d), the Sherwood number Sh is plotted when the bulk Damköhler number is $\mathrm{Da_b} = 10^8$ for (c) various values of the surface Damköhler number $\mathrm{Da_s}$ as a function of Pe and (d) various values of Pe as a function of $\mathrm{Da_s}$. In panel (c), the transition from a scaling of Pe^0 to $\mathrm{Pe}^{1/3}$ as the diffusion-limited regime is reached in the presence of strong bulk reaction is demonstrated. The limiting values of Sh shown in panel (b) are also shown with the same line styles in panels (a,c). The stoichiometry considered here is $(n, m, p, q) = (1, 2, 1, 2)$.

$\mathrm{Sh}(\mathrm{Pe} \gg 1, \mathrm{Da_b}, \mathrm{Da_s} \gg 1) \sim \mathrm{Pe}^{1/3}$ only when $\mathrm{Da_b} = 0$, i.e. the original Graetz Lévêque case, or when $\mathrm{Da_b} \to \infty$. At intermediate $\mathrm{Da_b}$, the scaling becomes nontrivial, because

it was previously demonstrated that the factor $f(\mathrm{Pe}, \mathrm{Da_s})$ depends on $\mathrm{Da_{b,eff}} = \mathrm{Da_b} L_{\mathrm{BL}}^2 \sim \mathrm{Da_b Pe}^{-2/3}$. In figure 4(b), Sh is plotted against $\mathrm{Da_s}$ at a fixed value of $\mathrm{Pe} = 10^5$. When $\mathrm{Da_s} \ll 1$, i.e. the reaction-limited regime, $\mathrm{Sh} \approx \mathrm{Da_s}$, regardless of $\mathrm{Da_b}$, as previously stated in equation (16). On the other hand, when $\mathrm{Da_s} \gg 1$, $\mathrm{Sh} \approx f(\mathrm{Pe}, \mathrm{Da_b})\mathrm{Sh_{GL}}$, where $f \approx 1$ when $\mathrm{Da_b} \approx 0$ and $f \approx 1/2$ when $\mathrm{Da_b} \to \infty$, as previously shown.

In figure 4(c,d), we now focus on the case of strong bulk reaction and we set $\mathrm{Da_b} = 10^8$. In figure 4(c), the Sherwood number Sh is plotted against the Péclet number Pe for various values of the surface Damköhler number. We observe that a transition from $\mathrm{Sh} \sim \mathrm{Pe}^0$ to $\mathrm{Sh} \sim \mathrm{Pe}^{1/3}$ is achieved as $\mathrm{Da_s}$ is increased. This is analogous to the transition that is observed in the absence of bulk reaction. Note that this is equivalent to a transition from $\sim \mathrm{Pe}^{-1}$ to $\sim \mathrm{Pe}^{-2/3}$ in terms of the % utilization, based on equation (11). In figure 4(d), Sh is plotted against $\mathrm{Da_s}$ for various Pe, showing the enhancement of mass transfer due to flow in the presence of strong bulk reaction.

The agreement between our two-dimensional simulations and our approximation in equation (21) in figure 4 gives us confidence that our approach is valid. In particular, at intermediate values of $\mathrm{Da_s}$, where our approximation is not formally valid, the agreement between our simulations and approximation demonstrates that the resistances to mass transfer are independent of one another, even in the presence of bulk reaction. This implies that the addition of bulk reaction only acts to modify the mass transfer resistance due to flow and not the mass transfer resistance due to finite surface reaction.

3.3 Mitigation strategy in $\mathrm{CO_2}$ reduction in aqueous flow reactors

In the previous subsection, we demonstrated that equation (21) provides a good approximation for the model problem defined by equations (7a)-(7e). Specifically, we found that in the presence of a competing bulk reaction, the mass transfer of the reactant to the surface in the diffusion-limited regime is given by simply scaling the Graetz Lévêque result by the reaction factor $f(\mathrm{Pe}, \mathrm{Da_b})$. With the stoichiometry given by $(n, m, p, q) = (1, 2, 1, 2)$,

this model problem corresponds to the problem of CO_2 saturated water undergoing the CO evolution reaction at the reactive surface. In the limit of strong bulk reaction, as is the case in CO_2 reduction, we showed that the presence of the species $X_2 = OH^-$ can deplete the Sherwood number for the species $X_1 = CO_2$ by a factor of 1/2. In practice, however, CO_2 reduction in a flow reactor is not performed using pure water. Typically, a buffered electrolyte, such as $KHCO_3$, is used to control the pH of the liquid near the reactive surface, and thus, improve the mass transfer of CO_2 to the reactive surface. In this subsection, we demonstrate the effect of a buffered electrolyte on mass transfer of CO_2 in an aqueous flow reactor, and discuss the relation of this realistic problem with our model problem.

Table 1: Constants associated with the $KHCO_3$ electrolyte

Parameter	Value	Units	Ref.
Reaction rates			
k_{1f}	8.42×10^3	$\mathrm{L\,mol^{-1}\,s^{-1}}$	41
k_{1r}	1.97×10^{-4}	$\mathrm{s^{-1}}$	39
k_{2f}	3.71×10^{-2}	$\mathrm{s^{-1}}$	39
k_{2r}	8.697×10^4	$\mathrm{L\,mol^{-1}\,s^{-1}}$	39
k_{3f}	1.254×10^6	$\mathrm{s^{-1}}$	39
k_{3r}	6.0×10^9	$\mathrm{L\,mol^{-1}\,s^{-1}}$	39
k_{4f}	1.242×10^{12}	$\mathrm{L\,mol^{-1}\,s^{-1}}$	39
k_{4r}	59.44	$\mathrm{s^{-1}}$	39
k_{5f}	2.3×10^{10}	$\mathrm{L\,mol^{-1}\,s^{-1}}$	45
k_{5r}	2.3×10^{-4}	$\mathrm{mol\,L^{-1}\,s^{-1}}$	39
Diffusivities			
D_{CO_2}	1.91×10^{-9}	$\mathrm{m^2\,s^{-1}}$	39
D_{OH^-}	5.29×10^{-9}	$\mathrm{m^2\,s^{-1}}$	39
D_{H^+}	9.311×10^{-9}	$\mathrm{m^2\,s^{-1}}$	39
$D_{CO_3^{2-}}$	0.92×10^{-9}	$\mathrm{m^2\,s^{-1}}$	39
$D_{HCO_3^-}$	1.185×10^{-9}	$\mathrm{m^2\,s^{-1}}$	39

The $KHCO_3$ electrolyte is governed by the reactions,[39]

$$CO_2 + OH^- \underset{k_{1r}}{\overset{k_{1f}}{\rightleftharpoons}} HCO_3^-, \tag{23}$$

$$CO_2 + H_2O \underset{k_{2r}}{\overset{k_{2f}}{\rightleftharpoons}} HCO_3^- + H^+, \tag{24}$$

$$CO_3^{2-} + H_2O \underset{k_{3r}}{\overset{k_{3f}}{\rightleftharpoons}} HCO_3^- + OH^-, \tag{25}$$

$$CO_3^{2-} + H^+ \underset{k_{4r}}{\overset{k_{4f}}{\rightleftharpoons}} HCO_3^-, \tag{26}$$

$$OH^- + H^+ \underset{k_{5r}}{\overset{k_{5f}}{\rightleftharpoons}} H_2O, \tag{27}$$

where the rate constants k_{if} and k_{ir} are given in table 1. Note that the simple reaction that motivated our model problem, discussed in §1, is the sum of the reactions given in equations (23) and (25); since the reaction given in equation (25) is relatively much faster, the reaction given in equation (23) controls the rate in that case. The equilibrium reaction constant for the simple reaction in our model problem, given previously in equation (1a) is $K_{eq} = k_{1f}k_{3r}/k_{1r}k_{3f} = O(10^{11})\ \mathrm{L}^2/\mathrm{mol}^2$. Without a buffered electrolyte, typical concentrations of CO_2 and OH^- near the cathode are driven out of equilibrium due to the production of OH^- and are both $O(.01)\ \mathrm{mol\,L^{-1}}$. Since the concentration of CO_3^{2-} is expected to be much less than what would be expected in the corresponding equilibrium – $O(10^5)\ \mathrm{mol\,L^{-1}}$ – the reverse reaction is thus negligible relative to the forward reaction, justifying our neglect of the reverse reaction in our model problem. This argument is no longer valid, however, with the addition of $KHCO_3$, and thus both forward and reverse reactions need to be considered here. The benefit of adding $KHCO_3$ is summarized in figure 5(a): (1) First, the CO evolution reaction produces 2 OH^- molecules for each CO_2 molecule consumed. (2) Next, the OH^- then reacts with either CO_2 to form HCO_3^- via equation (23) or with HCO_3^- to form CO_3^{2-} and H_2O via equation (25). (3) Finally, since a fraction of the OH^- has been consumed by the added HCO_3^-, more CO_2 is allowed to reach the reactive surface.

We simulate the model problem as before, but now with the addition of $KHCO_3$. There

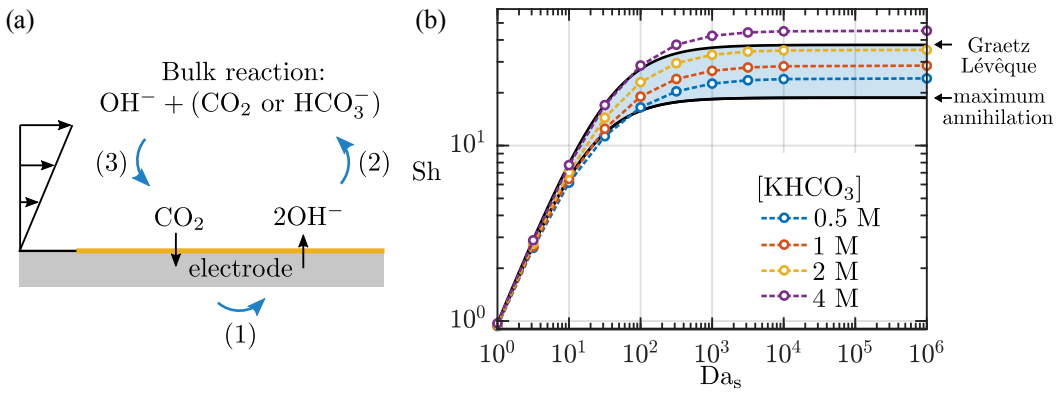

Figure 5: (a) Schematic demonstrating the effect of adding $KHCO_3$. (1) 2 OH^- molecules are produced for each CO_2 molecule consumed at the surface. (2) The OH^- then reacts away some of either the CO_2 or HCO_3^- present in the bulk. (3) Since the presence of HCO_3^- partially reacts away some of the OH^-, more CO_2 is allowed to reach the reactive surface. (b) The Sherwood number is plotted as a function of the surface Damköhler number Da_s for various electrolyte strengths $[KHCO_3] = \{0.5, 1, 2, 4\}$ M when $Pe = 10^5$. The light blue band indicates the band of possible Sh for our model problem given by equation (21): $Da_b = \infty$ corresponds to the lower bound and $Da_b = 0$ corresponds to the Graetz Lévêque upper bound.

are now five species, $X_i \in \{CO_2, OH^-, HCO_3^-, CO_3^{2-}, H^+\}$, governed by the coupled advection-diffusion-reaction equations for each species X_i,

$$\mathrm{Pe}\, y\frac{\partial C_i}{\partial x} = \alpha_i\left(\frac{\partial^2 C_i}{\partial x^2} + \frac{\partial^2 C_i}{\partial y^2}\right) + R_i(\{C_j\}), \qquad x, y \geq 0, \quad (28a)$$

$$C_i = C_i^{\mathrm{eq}}/C_{\mathrm{CO_2}}^{\mathrm{eq}}, \qquad \text{at } x = 0, \quad (28b)$$

$$\frac{\partial C_{\mathrm{CO_2}}}{\partial y} = \mathrm{Da_s} C_{\mathrm{CO_2}}, \frac{\partial C_{\mathrm{OH^-}}}{\partial y} = -2\frac{\mathrm{Da_s}}{\alpha_{\mathrm{OH^-}}} C_{\mathrm{CO_2}}, \frac{\partial C_{\{\mathrm{HCO_3^-}, \mathrm{CO_3^{2-}}, \mathrm{H^+}\}}}{\partial y} = 0, \qquad \text{at } y = 0, \quad (28c)$$

$$C_i = C_i^{\mathrm{eq}}/C_{\mathrm{CO_2}}^{\mathrm{eq}}, \qquad \text{at } y = \infty, \quad (28d)$$

where $\alpha_i = D_i/D_{\mathrm{CO_2}}$ are diffusivity ratios, $R_i(\{C_j\})$ are dimensionless forward and reverse reaction rates based on reactions in equations (23)-(27), and C_i^{eq} are dimensional concentrations of species i at chemical equilibrium. We choose a cathode length of $L = 1$ cm and concentrations are nondimensionalized here using $C_{\mathrm{CO_2}}^{\mathrm{eq}} = 34$ mM; this nondimensionalization is consistent with our model problem, where the only nonzero bulk concentration was

C_1^∞. The diffusivities D_i are tabulated in table 1. Note that in contrast to the model problem, we now consider the more realistic case of unequal diffusivities; previously in our model problem, it was assumed that the boundary layer of the second species could not exceed that of the primary species – that assumption is no longer valid here. Additionally, note that there are now multiple bulk Damköhler numbers, due to the inclusion of the forward and reverse reactions given in equations (23)-(27), in contrast to the single forward bulk reaction in our model problem.

In figure 5(b), we calculate Sh as a function of the surface Damköhler number $\mathrm{Da_s}$ for various electrolyte strengths $[\mathrm{KHCO_3}] = \{0.5, 1, 2, 4\}$ M for a fixed value of $\mathrm{Pe} = 10^5$. The light blue band indicates the band of possible Sh for our model problem given by equation (21): $\mathrm{Da_b} = \infty$ corresponds to the lower bound and $\mathrm{Da_b} = 0$ corresponds to the Graetz Lévêque upper bound. We observe that when $[\mathrm{KHCO_3}]$ approaches 0 M, we approximately approach the lower bound given by our model problem. Of course, this is not the exact lower bound for the problem with $[\mathrm{KHCO_3}]$, because our model problem did not include the effect of unequal diffusivities. As $[\mathrm{KHCO_3}]$ increases, we observe that Sh increases as more of the $\mathrm{OH^-}$ is consumed by the buffer and more $\mathrm{CO_2}$ is allowed to reach the reactive surface. As posed, Sh can exceed the Graetz Lévêque limit at high $[\mathrm{KHCO_3}]$ as the reverse rate of the reaction given in equation (23) can exceed the forward rate within the boundary layer. However, when converting back to dimensional units, it is important to note that the flux is constrained by the chemical constraint that the solubility of $\mathrm{CO_2}$ decreases exponentially with increasing $[\mathrm{KHCO_3}]$ via the Sechenov equation[46,47] – an effect that we have not included here. Despite these limitations, this example thus illustrates the utility of our approximation from our model problem, even in a situation where the chemistry is far more complex.

4 Concluding remarks

In this work, we have studied how the mass transfer of a species in shear flow is affected by the production of a second species that partially reacts away the first species, where the second species is produced at the surface with the first species as the reactant. We have considered general stoichiometry, but our model problem is motivated by electrochemical CO_2 reduction in aqueous flow reactors. By considering the various resistances to mass transfer, we derived a simple approximation of the Sherwood number Sh, a dimensionless mass flux, as a function of the Péclet number Pe, the surface Damköhler number $\mathrm{Da_s}$, and the bulk Damköhler number $\mathrm{Da_b}$. Instead of a full simulation of equations (7a)-(7e), our approximation only requires the numerical solution of the one-dimensional problem given by equations (19a)-(19d); approximate solutions for the cases where $\mathrm{Da_{b,eff}} \ll 1$ and $\mathrm{Da_{b,eff}} \to \infty$ are also given in equation (22). We then successfully compared our approximation with numerical solutions of the governing advection-diffusion-reaction equation. Notably, we found that when strong surface reaction is present, the surface flux of the reactant, i.e. the Sherwood number Sh, is well described by the Graetz Lévêque result reduced by a reaction factor $f(\mathrm{Pe}, \mathrm{Da_b})$ due to the competing bulk reaction. With the stoichiometry relevant to electrochemical CO_2 reduction, this reaction factor $f(\mathrm{Pe}, \mathrm{Da_b})$ is simply $1/2$ in the diffusion-limited regime when $\mathrm{Da_{b,eff}} \gg 1$.

While the theory developed in this work has been developed generally, here, we emphasize the strong connection between our transport theory and experiments. In an experiment, the flow rate Q is set by a pump, and the corresponding shear rate $\dot{\gamma}$ and Péclet number Pe can be calculated using the discussion following equation (11). Given that $\mathrm{Pe} \gg 1$, and under mass-transport limiting conditions, the Sherwood number can be estimated with equation (17) where $\mathrm{Sh_{GL}}$ is given by equation (13). As noted above, $f(\mathrm{Pe}, \mathrm{Da_b})$ is simply $1/2$ for most systems where $\mathrm{Da_{b,eff}} \gg 1$ (e.g., when $\mathrm{Pe} = 10^5$ for a $L = 1$ cm long cathode, $\mathrm{Da_{b,eff}} = 1.35 \times 10^4$). The dimensional flux J can then be calculated by redimensionalizing Sh via equation (9), and the CO current density, e.g., with units of $\mathrm{A/m^2}$, can then be

estimated by multiplying J with nF, where $n = 2$ represents the 2 electrons transferred per CO_2 molecule and F is Faraday's constant. This process then gives an idea of how the CO current density is expected to scale with the flow rate Q. If the experiment is not under mass-transport limiting conditions, then a prediction of Sh can be made with equation (21), where Da_s can be calculated with equations (6) and (3).

Even though our model problem provides a rough estimate of the CO_2 reduction rate, we recognize that CO_2 reduction is not conducted using pure water. Thus, we also considered the use of a buffered electrolyte, $KHCO_3$. This is a common strategy employed in experiments to control the pH, and thus the concentration of the OH^- annihilator in the microenvironment near the cathode surface. While our results provide insight into how the addition of a buffered electrolyte can improve CO_2 transfer, there are many possible extensions to this work that would be of interest. For example, it would be interesting to include the previously mentioned effect that the solubility of CO_2 decreases exponentially with increasing $[KHCO_3]$[46,47] and understand how $[KHCO_3]$ affects the dimensional flux of CO_2. Additionally, it is known that $[KHCO_3]$ shifts the reaction rate constants.[38,48,49] Furthermore, the ions present in the system are charged – an effect we have neglected; understanding the effect of electromigration on the ion transport, and ultimately on the CO_2 mass transfer, would be insightful. Finally, we conclude by highlighting one important extension that should be explored in future work: the effect of temperature on the reaction rate coefficients. In a realistic experimental system, the temperature of the liquid can vary spatially due to Ohmic heating or heat generated by the reactions. While we have assumed uniform room temperature in our present work, the forward reaction rate of the reaction given in equation (23) is known to depend on temperature. For example, Astarita et al.[41] reports the correlation $k_{1f} = \exp(31.3957 - 6665.9912/T)$ at infinite dilution, where T [K] is the temperature. As an example, the temperatures $T = 20°C$ and $T = 50°C$ correspond to $k_{1f} = 5.75 \times 10^3$ L mol^{-1} s^{-1} and $k_{1f} = 47.5 \times 10^3$ L mol^{-1} s^{-1}, respectively. Assuming a Péclet number of $Pe = 10^5$, these correspond to effective bulk Damköhler numbers of

$\mathrm{Da}_{\mathrm{b,eff}} = 0.92 \times 10^4$ and $\mathrm{Da}_{\mathrm{b,eff}} = 7.6 \times 10^4$, respectively. By looking at figure 3, we see that both of these values are close to the $\mathrm{Da}_{\mathrm{b,eff}} \to \infty$ asymptote that we reported, implying only a small change in Sh. While a full inclusion of temperature effects is out of scope of the current work, since this would require a coupled model of the heat transfer process via the advection-diffusion equation for heat and an understanding of the temperature dependence of all reactions, here we have demonstrated how our framework may take this into account in future work.

Acknowledgement

T.Y.L. thanks Dr. Thomas Moore for helpful discussions regarding bicarbonate chemistry and Drs. Marissa Wood and Jeremy Feaster for their insights on experimental flow reactors. This work was performed under the auspices of the U.S. Department of Energy by Lawrence Livermore National Laboratory under Contract DE-AC52-07NA27344. This work was also supported by the Lawrence Livermore National Laboratory LDRD SI 19-SI-005. This work was performed under the auspices of a cooperative research and development agreement between Lawrence Livermore National Laboratory, Stanford University, and TOTAL American Services, Inc. (affiliate of TOTAL SE) under agreement number TC02307. LLNL Release Number LLNL-JRNL-821360.

References

(1) Kibria, M. G.; Edwards, J. P.; Gabardo, C. M.; Dinh, C.-T.; Seifitokaldani, A.; Sinton, D.; Sargent, E. H. Electrochemical CO2 reduction into chemical feedstocks: from mechanistic electrocatalysis models to system design. *Advanced Materials* **2019**, *31*, 1807166.

(2) Verma, S.; Kim, B.; Jhong, H.-R. M.; Ma, S.; Kenis, P. J. A gross-margin model for

defining technoeconomic benchmarks in the electroreduction of CO2. *ChemSusChem* **2016**, *9*, 1972–1979.

(3) Nitopi, S.; Bertheussen, E.; Scott, S. B.; Liu, X.; Engstfeld, A. K.; Horch, S.; Seger, B.; Stephens, I. E.; Chan, K.; Hahn, C.; Norskov, J. K.; Jaramillo, T. F.; Chorkendorff, I. Progress and perspectives of electrochemical CO2 reduction on copper in aqueous electrolyte. *Chemical reviews* **2019**, *119*, 7610–7672.

(4) Obama, B. The irreversible momentum of clean energy. *Science* **2017**, *355*, 126–129.

(5) Rockström, J.; Gaffney, O.; Rogelj, J.; Meinshausen, M.; Nakicenovic, N.; Schellnhuber, H. J. A roadmap for rapid decarbonization. *Science* **2017**, *355*, 1269–1271.

(6) Haszeldine, R. S. Carbon capture and storage: how green can black be? *Science* **2009**, *325*, 1647–1652.

(7) Hatsukade, T.; Kuhl, K. P.; Cave, E. R.; Abram, D. N.; Jaramillo, T. F. Insights into the electrocatalytic reduction of CO 2 on metallic silver surfaces. *Physical Chemistry Chemical Physics* **2014**, *16*, 13814–13819.

(8) Higgins, D.; Hahn, C.; Xiang, C.; Jaramillo, T. F.; Weber, A. Z. Gas-diffusion electrodes for carbon dioxide reduction: a new paradigm. *ACS Energy Letters* **2018**, *4*, 317–324.

(9) Kuhl, K. P.; Cave, E. R.; Abram, D. N.; Jaramillo, T. F. New insights into the electrochemical reduction of carbon dioxide on metallic copper surfaces. *Energy & Environmental Science* **2012**, *5*, 7050–7059.

(10) Wicks, J.; Jue, M. L.; Beck, V. A.; Oakdale, J. S.; Dudukovic, N. A.; Clemens, A. L.; Liang, S.; Ellis, M. E.; Lee, G.; Baker, S. E.; Duoss, E. B.; Sargent, E. H. 3D-Printable Fluoropolymer Gas Diffusion Layers for CO2 Electroreduction. *Advanced Materials* **2021**, *33*, 2003855.

(11) Corral, D.; Feaster, J. T.; Sobhani, S.; DeOtte, J. R.; Lee, D. U.; Wong, A. A.; Hamilton, J.; Beck, V. A.; Sarkar, A.; Hahn, C.; Jaramillo, T. F.; Baker, S. E.; Duoss, E. B. Advanced manufacturing for electrosynthesis of fuels and chemicals from CO 2. *Energy & Environmental Science* **2021**, *14*, 3064–3074.

(12) De Arquer, F. P. G.; Dinh, C.-T.; Ozden, A.; Wicks, J.; McCallum, C.; Kirmani, A. R.; Nam, D.-H.; Gabardo, C.; Seifitokaldani, A.; Wang, X.; Li, Y. C.; Li, F.; Edwards, J.; Richter, L. J.; Thorpe, S. J.; Sinton, D.; Sargent, E. H. CO2 electrolysis to multicarbon products at activities greater than 1 A cm- 2. *Science* **2020**, *367*, 661–666.

(13) Weng, L.-C.; Bell, A. T.; Weber, A. Z. Towards membrane-electrode assembly systems for CO 2 reduction: a modeling study. *Energy & Environmental Science* **2019**, *12*, 1950–1968.

(14) Pérez-Gallent, E.; Sánchez-Martínez, C.; Geers, L. F.; Turk, S.; Latsuzbaia, R.; Goetheer, E. L. Overcoming Mass Transport Limitations in Electrochemical Reactors with a Pulsating Flow Electrolyzer. *Industrial & Engineering Chemistry Research* **2020**, *59*, 5648–5656.

(15) Bui, J. C.; Kim, C.; Weber, A. Z.; Bell, A. T. Dynamic Boundary Layer Simulation of Pulsed CO2 Electrolysis on a Copper Catalyst. *ACS Energy Letters* **2021**, *6*, 1181–1188.

(16) Kopljar, D.; Inan, A.; Vindayer, P.; Wagner, N.; Klemm, E. Electrochemical reduction of CO 2 to formate at high current density using gas diffusion electrodes. *Journal of Applied Electrochemistry* **2014**, *44*, 1107–1116.

(17) Li, Y. C.; Lee, G.; Yuan, T.; Wang, Y.; Nam, D.-H.; Wang, Z.; García de Arquer, F. P.; Lum, Y.; Dinh, C.-T.; Voznyy, O.; Sargent, E. H. CO2 electroreduction from carbonate electrolyte. *ACS Energy Letters* **2019**, *4*, 1427–1431.

(18) Weekes, D. M.; Salvatore, D. A.; Reyes, A.; Huang, A.; Berlinguette, C. P. Electrolytic CO2 reduction in a flow cell. *Accounts of chemical research* **2018**, *51*, 910–918.

(19) Bortels, L.; Deconinck, J.; Van Den Bossche, B. The multi-dimensional upwinding method as a new simulation tool for the analysis of multi-ion electrolytes controlled by diffusion, convection and migration. Part 1. Steady state analysis of a parallel plane flow channel. *Journal of Electroanalytical Chemistry* **1996**, *404*, 15–26.

(20) Parrish, W. R.; Newman, J. Current distributions on plane, parallel electrodes in channel flow. *Journal of the Electrochemical Society* **1970**, *117*, 43.

(21) Zhang, Z.; Melo, L.; Jansonius, R. P.; Habibzadeh, F.; Grant, E. R.; Berlinguette, C. P. pH matters when reducing CO2 in an electrochemical flow cell. *ACS Energy Letters* **2020**, *5*, 3101–3107.

(22) Dinh, C.-T.; Burdyny, T.; Kibria, M. G.; Seifitokaldani, A.; Gabardo, C. M.; De Arquer, F. P. G.; Kiani, A.; Edwards, J. P.; De Luna, P.; Bushuyev, O. S.; Zou, C.; Quintero-Bermudez, R.; Pang, Y.; Sinton, D.; Sargent, E. H. CO2 electroreduction to ethylene via hydroxide-mediated copper catalysis at an abrupt interface. *Science* **2018**, *360*, 783–787.

(23) Newman, J. Extension of the Lévêque solution. *Journal of Heat Transfer* **1969**, 177–178.

(24) Graetz, v. L. Ueber die wärmeleitungsfähigkeit von flüssigkeiten. *Annalen der Physik* **1882**, *254*, 79–94.

(25) Lévêque, A. Les lois de la transmission de chaleur par convection. *Annales des Mines* **1928**, *13*, 201–299, 305–362, 381–415.

(26) Phillips, C. G. Heat and mass transfer from a film into steady shear flow. *The Quarterly Journal of Mechanics and Applied Mathematics* **1990**, *43*, 135–159.

(27) Stone, H. A. Heat/mass transfer from surface films to shear flows at arbitrary Peclet numbers. *Physics of Fluids A: Fluid Dynamics* **1989**, *1*, 1112–1122.

(28) Shah, P. N.; Shaqfeh, E. S. Heat/mass transport in shear flow over a heterogeneous surface with first-order surface-reactive domains. *Journal of Fluid Mechanics* **2015**, *782*, 260.

(29) Shah, P. N.; Lin, T. Y.; Shaqfeh, E. S. Heat/mass transport in shear flow over a reactive surface with inert defects. *Journal of Fluid Mechanics* **2017**, *811*, 372–399.

(30) Chambré, P. L.; Acrivos, A. On chemical surface reactions in laminar boundary layer flows. *Journal of Applied Physics* **1956**, *27*, 1322–1328.

(31) Acrivos, A.; Chambre, P. L. Laminar boundary layer flows with surface reactions. *Industrial & Engineering Chemistry* **1957**, *49*, 1025–1029.

(32) Juhasz, N. M.; Deen, W. M. Effect of local Peclet number on mass transfer to a heterogeneous surface. *Industrial & engineering chemistry research* **1991**, *30*, 556–562.

(33) Apelblat, A. Mass transfer with a chemical reaction of the first order: analytical solutions. *The chemical Engineering journal* **1980**, *19*, 19–37.

(34) Friedlander, S.; Litt, M. Diffusion controlled reaction in a laminar boundary layer. *Chemical Engineering Science* **1958**, *7*, 229–234.

(35) Acrivos, A. On laminar boundary layer flows with a rapid homogeneous chemical reaction. *Chemical Engineering Science* **1960**, *13*, 57–62.

(36) Friedlander, S.; Keller, K. The structure of the zone of diffusion controlled reaction. *Chemical Engineering Science* **1963**, *18*, 365–375.

(37) Den Hartog, H.; Beek, W. Local mass transfer with chemical reaction. *Applied Scientific Research* **1968**, *19*, 311–337.

(38) Borhani, T. N. G.; Azarpour, A.; Akbari, V.; Alwi, S. R. W.; Manan, Z. A. CO2 capture with potassium carbonate solutions: A state-of-the-art review. *International journal of greenhouse gas control* **2015**, *41*, 142–162.

(39) Weng, L.-C.; Bell, A. T.; Weber, A. Z. Modeling gas-diffusion electrodes for CO 2 reduction. *Physical Chemistry Chemical Physics* **2018**, *20*, 16973–16984.

(40) Ma, M.; Clark, E. L.; Therkildsen, K. T.; Dalsgaard, S.; Chorkendorff, I.; Seger, B. Insights into the carbon balance for CO 2 electroreduction on Cu using gas diffusion electrode reactor designs. *Energy & Environmental Science* **2020**, *13*, 977–985.

(41) Astarita, G.; Savage, D.; Bisio, A. *Gas Treating with Chemical Solvents*; A Wiley-Interscience publication; John Wiley, 1983.

(42) Fukunaka, Y.; Jiang, M.; Yamamoto, T.; Asaki, Z.; Kondo, Y. Nonuniformity of NaOH concentration and effective bubble diameter in CO 2 injection into aqueous NaOH solution. *Metallurgical Transactions B* **1989**, *20*, 5–12.

(43) Churchill, S.; Usagi, R. A general expression for the correlation of rates of transfer and other phenomena. *AIChE Journal* **1972**, *18*, 1121–1128.

(44) Gupta, N.; Gattrell, M.; MacDougall, B. Calculation for the cathode surface concentrations in the electrochemical reduction of CO 2 in KHCO 3 solutions. *Journal of applied electrochemistry* **2006**, *36*, 161–172.

(45) Schulz, K. G.; Riebesell, U.; Rost, B.; Thoms, S.; Zeebe, R. Determination of the rate constants for the carbon dioxide to bicarbonate inter-conversion in pH-buffered seawater systems. *Marine chemistry* **2006**, *100*, 53–65.

(46) Schumpe, A. The estimation of gas solubilities in salt solutions. *Chemical engineering science* **1993**, *48*, 153–158.

(47) Weisenberger, S.; Schumpe, d. A. Estimation of gas solubilities in salt solutions at temperatures from 273 K to 363 K. *AIChE Journal* **1996**, *42*, 298–300.

(48) Cents, A.; Brilman, D. W. F.; Versteeg, G. CO2 absorption in carbonate/bicarbonate solutions: The Danckwerts-criterion revisited. *Chemical Engineering Science* **2005**, *60*, 5830–5835.

(49) Kaur, H.; Chen, C.-C. Thermodynamic modeling of CO2 absorption in aqueous potassium carbonate solution with electrolyte NRTL model. *Fluid Phase Equilibria* **2020**, *505*, 112339.

Graphical TOC Entry